

Supporting information for: Imaging the Indian Subcontinent beneath the Himalaya

Vera Schulte-Pelkum, Gaspar Monsalve, Anne Sheehan, Som Sapkota, M. R. Pandey, Roger Bilham, & Francis Wu

Receiver function calculation and data selection

All recorded teleseismic events with $m_b \geq 5.0$ within P , PP , and PKP distance ranges based on the NEIC catalogue were checked automatically for their suitability for receiver function analysis. For all records where the direct P arrival showed a minimum signal-to-noise ratio of 3 on the vertical component, receiver functions were calculated using a time-domain iterative method [1] and those with a variance reduction of at least 70% were retained for analysis. The automated selection eliminated the majority of the initial events (including most of the events in the PP , and all but a handful in the PKP distance ranges) and left only high-quality receiver functions and a few outliers per station, which were removed at visual inspection. Typically, transverse component receiver functions are noisier, and fewer are retained based on the variance reduction criterion during the automatic processing than the number of radial receiver functions at the same station. Three southern Nepal stations situated on thick sediments (BIRA, JANA, GAIG) that displayed receiver functions strongly dominated by sediment multiples were excluded from the common point conversion stack. Most stations in Tibet yielded sparser data than those in Nepal due to limited accessibility (less frequent servicing).

Anisotropic layer

We discuss the azimuthal sections in Figure 3 in the main paper in further detail. The timing of the arrivals is slowness corrected to represent vertical incidence. In Figure 3a, note the phase with polarity reversal at 1.6 s on the radial component. The transverse component shows arrivals with polarity reversals at 0.6 and 1.6 s. Azimuthal variation of receiver functions can be caused by several different subsurface features, such as dipping isotropic interfaces, scattering, anisotropy, and other lateral variations. A polarity reversal on the radial component requires strong anisotropy; the periodicity of 360 degrees indicates a steeply plunging symmetry axis. While an arrival at 0.6 s on the radial component is mostly obscured by direct P , paired arrivals with reversed polarity are clearly visible on the transverse component and originate from the top and bottom of a layer of only a few km thickness. Figure 3b shows synthetics [2] that match the observed pattern at stations SIND in Figure 3a. The synthetic receiver functions are calculated for the average observed slowness and a moveout correction is applied in the same way as to the data. Parameters for the synthetic model are as follows (for the symmetry axis, in this case a slow axis as defined by the negative P and S anisotropy, strike is clockwise from North, and plunge is positive down from strike azimuth):

Supplementary Table 1: model with anisotropic and sediment layers used to produce synthetics

thickness	ρ	v_p	v_s	% v_p	% v_s	strike	plunge	η
km	g/cm ³	km/s	km/s			deg	deg	
2	2.5	4.0	1.6	0	0			
6	2.9	5.4	2.8	-20	-20	18	-50	0.4
∞	3.2	6.5	3.7	0	0			

The forward modelling is nonunique, as tradeoffs exist between layer thicknesses and velocities, and between anisotropy magnitude and velocity contrasts. Required features to model the arrivals between 0 and 2 s are strong anisotropy ($\geq 15\%$), slow symmetry (i.e., planes of high velocity perpendicular to a slow symmetry axis), alignment of the azimuth of the symmetry axis with the NNE direction normal to the Himalayan arc, a steep dip of the fast planes down towards NNE, and an anisotropic shape parameter η (which describes the distortion of the phase velocity surface from an ellipsoid) at the lower end of the range typical for anisotropic crustal materials (0.4-0.9) [3]. While the polarity pattern in the radial and tangential components is generated by the thin anisotropic layer in an otherwise homogeneous halfspace, we have added a sedimentary layer above it to improve the match in the waveforms. The sedimentary layer is also required by geology (station SIND is located on the Siwaliks sediments) and for matching SIND arrivals to nearby stations. Arrivals after 2 s display additional azimuthal complexity not explained by the influence of the shallow anisotropic layer alone, and they are not modeled in the synthetics.

Figure 3c clearly shows the conversion from the bottom of the anisotropic layer at station BUNG, situated 70 km north of station SIND. The topside conversion at BUNG is less clear than at SIND, where there is a large contrast to overlying sediments (BUNG has fast shallow velocities rather than a surface sedimentary layer, see section below). Similar azimuthal patterns are seen at all stations in Nepal. The areal extent of station locations with similar arrivals further supports the presence of a continuous anisotropic layer as the cause, rather than lateral heterogeneities. Our data are insufficient to confirm or exclude continuation of the layer into Tibet, mostly due to reduced data coverage, but also because the arrivals are later and more prone to modification by shallower structure. However, Figure 2c suggests that the decollement shear zone may persist under Tibet, and the hint of its presence we see corresponds well to the decollement imaged by INDEPTH reflection data (Figure 2d).

High-velocity anomaly at BUNG

The azimuthal variations are observed at all stations and render a standard analysis of moveout with azimuthal averaging nearly meaningless. Only a few stations have a sufficient number of receiver functions with a range of slownesses in a narrow azimuthal range to allow a moveout analysis. We show an example for station BUNG in Figure S1. Moho and midcrustal arrivals appear early at BUNG compared to surrounding stations. Matching the midcrustal multiple

requires a high-velocity anomaly above 20 km depth, which brings the single midcrustal and Moho conversion in line with that observed at surrounding stations.

Common conversion point stack and velocity model for depth migration

SIND, located on the Siwaliks sediments, and BUNG, on top of the high-velocity anomaly, were the only stations we applied shallow velocity corrections to in the common conversion point stack in Figure 2. Depth migration for all other stations were performed with separate 1-D models for Nepal and Tibet, obtained from tomographic inversion of local and regional events (Monsalve et al., manuscript in preparation). Starting models for the inversions were 1-D models for Nepal [4] and Tibet [5]. Final models are close to the initial one for Nepal, but significantly faster in the lower crust for Tibet. The models are as follows:

Supplementary Table 2: tomographic inversion velocity models

depth km	v_p km/s	v_s km/s
Nepal		
20	5.7	3.3
48	6.3	3.7
∞	8.1	4.7
Tibet		
40	5.5	3.4
75	7.4	4.3
∞	8.1	4.7

Elevation correction is performed assuming surface velocities above sea level of $v_p = 5.5$ km/s, $v_s = 3.2$ km/s. Elevation correction times are small in Nepal (a few tenths of a second for stations in the Lesser Himalaya) and reach 1.6 s for the highest station in Tibet (RBSH).

A faint arrival with apparent southward dip between 70 and 80 km in Nepal is likely a midcrustal multiple. The midcrustal arrival in Nepal dips to the north from 17 km to 20 km depth. The opposite (southward) apparent dip of the midcrustal multiple is due to increasing sediment thickness from north to south. The direct arrival converts at the midcrustal interface and traverses the sediment layer once. However, the midcrustal multiple bounces once between the surface and the midcrustal interface, traversing the sediment layer twice more. The midcrustal multiple therefore experiences a disproportionately longer delay than the direct midcrustal arrival the thicker the sediment, and therefore appears later at southern stations, causing the reversed dip. We tested this behaviour through forward modelling.

Validation of single profile treatment of extended network data

Since our network had about equal E–W and N–S aperture, there exists the possibility of structural variations perpendicular to our profile that would render the single profile treatment invalid. In order to test for the influence of lateral variations on our results, we calculated the same stacks using only the eastern and the western half of the network, respectively. The resulting stacks (Figure S2) show good agreement and prove that we can neglect arc-perpendicular variations to first order. This finding is also corroborated by E–W profile stacks of data from subgroups of stations, which show no significant E–W variations.

Azimuthal difference stack

In order to image arrivals with polarity reversals over backazimuth that cancel out in the standard stacking technique [6] which adds amplitudes from all backazimuths, we modified the technique as follows. At each station, we calculate the median radial receiver function for the northern quadrants and the southern quadrants respectively, after correcting for slowness. The northern median receiver function is subtracted from the southern one. We then take half the amplitude of the difference receiver function, and project it back along the individual raypaths of the initial receiver functions. The stacking procedure is then performed as usual including the standard elevation correction.

Fast seismic velocities in the lower Tibetan crust

While the tomographic inversion results are the subject of a separate paper (Monsalve et al., manuscript in preparation), the necessity for a fast lower crustal velocity under the Tibetan plateau is a robust feature. Figure S3 shows a Wadati diagram for an example event. A Wadati diagram plots $S - P$ arrival time as a function of P arrival time at each station. A least-squares fit of a line through the arrivals intersects the x-axis ($S - P$ time of zero) at the best fit origin time. The event is then located with a given velocity model [5]. The location selects a hypocenter and origin time that minimize the P and S arrival time residuals. Using the model, location, and origin time, theoretical P and S arrival times are calculated for each station and added to the Wadati diagram, where they lie on a perfect line. A difference in slope of the theoretical versus the best fit lines indicates that the model's P to S velocity ratio is incorrect. A difference in the origin times indicates that the model is too fast (theoretical origin time later than best fit origin time) or too slow (best fit origin time later than theoretical origin time). The latter is the case in the example in Figure S3.

We perform these calculations for all events under the Tibetan Plateau and plot the resulting origin time biases in Figure S4. Each point represents an event with at least six P and S arrival time pairs picked. Events below 40 km depth have a negative origin time bias, indicating that the model's lower crust, with P and S velocities of 6.5 and 3.8 km/s respectively [5], is too slow. The upper crust appears slightly too fast. The tomographic inversion returns velocities that are

in agreement with these observations, with a slower upper crust and a significantly faster lower crust. The lower crustal velocities (v_p of 7.4 km/s) are fast even for mafic crust at temperature and pressure conditions typical for 40 to 75 km depth [7], but can be easily achieved if some of the material has been converted to eclogite.

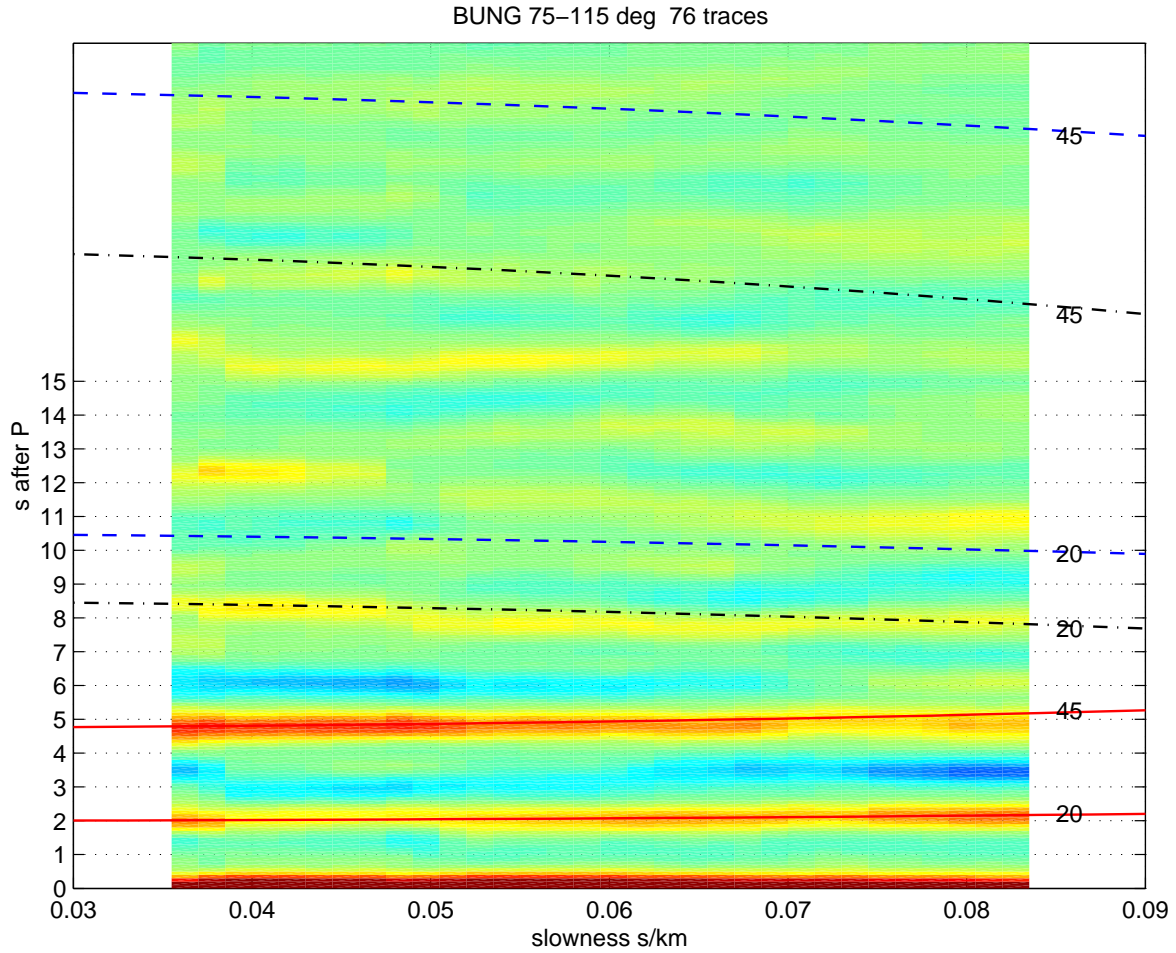
Wadati and origin time plots for Nepal and the High Himalaya reveal no unusually fast velocities in the lower crust, supporting our conclusion that the fast material is generated under Tibet through eclogitization, rather than being preexistent in the Indian crust before subduction.

We discuss in the main paper an expected volume reduction of up to 6% in the lower Indian crust. The thickness of the crust between the decollement and the Moho does not decrease visibly going from the High Himalaya to the zone with partial eclogitisation in Figure 2d. This may be partly due to uncertainty in the depth of the decollement. Our receiver function analysis did not allow us to image it robustly in that section of the profile, as the shear zone in Figure 2c shows up only faintly, if at all, under most of Tibet. The INDEPTH reflection section was modified from [8] and therefore migrated from time to depth with a slightly different velocity model than our receiver function profile. Last, we cannot exclude additional thickness changes in the lower crust due to ductile deformation.

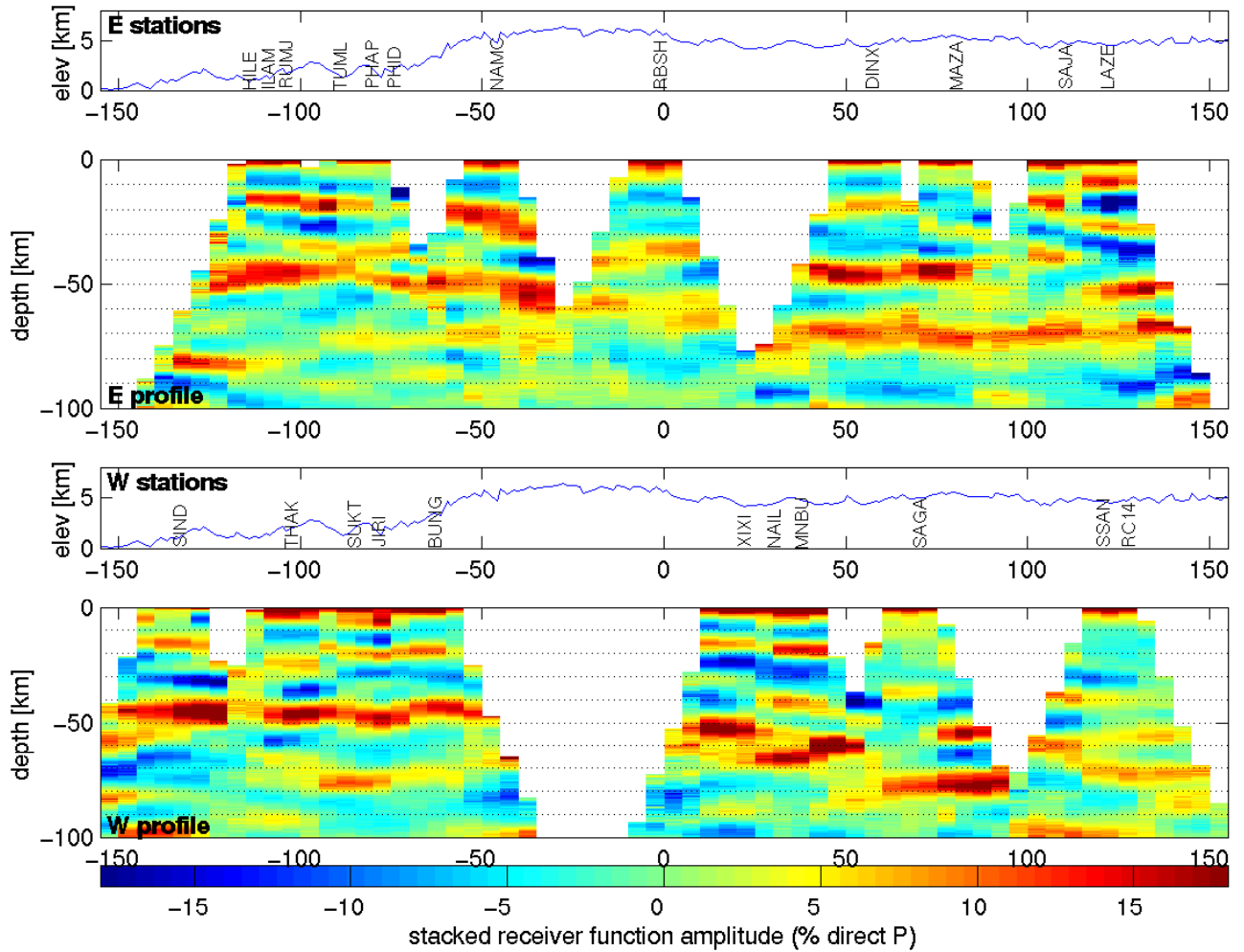
References

- [1] Ligorria-J-P & Ammon, C. J. Iterative deconvolution and receiver-function estimation. *Bull. Seismol. Soc. Am.* **89**, 1395–1400 (1999).
- [2] Frederiksen, A. & Bostock, M. Modelling teleseismic waves in dipping anisotropic structures. *Geophys. J. Int.* **141**, 401–412 (2000).
- [3] Godfrey, N. J., Christensen, N. & Okaya, D. Anisotropy of schists: Contribution of crustal anisotropy to active source experiments and shear wave splitting observations. *J. Geophys. Res.* **105**, 27,991–28,007 (2000).
- [4] Pandey, M. R., Tandukar, R. P., Avouac, J.-P., Lave, J. & Massot, J.-P. Interseismic strain accumulation on the Himalayan crustal ramp (Nepal). *Geophys. Res. Lett.* **22**, 751–754 (1995).
- [5] Cotte, N. *et al.* Determination of the crustal structure in southern Tibet by dispersion and amplitude analysis of Rayleigh waves. *Geophys. J. Int.* **138**, 809–819 (1999).
- [6] Dueker, K. G. & Sheehan, A. F. Mantle discontinuity structure beneath the Colorado Rocky Mountains and High Plains. *J. Geophys. Res.* **103**, 7153–7169 (1998).
- [7] Christensen, N. & Mooney, W. Seismic velocity structure and composition of the continental crust: A global view. *J. Geophys. Res.* **100**, 9761–9788 (1995).

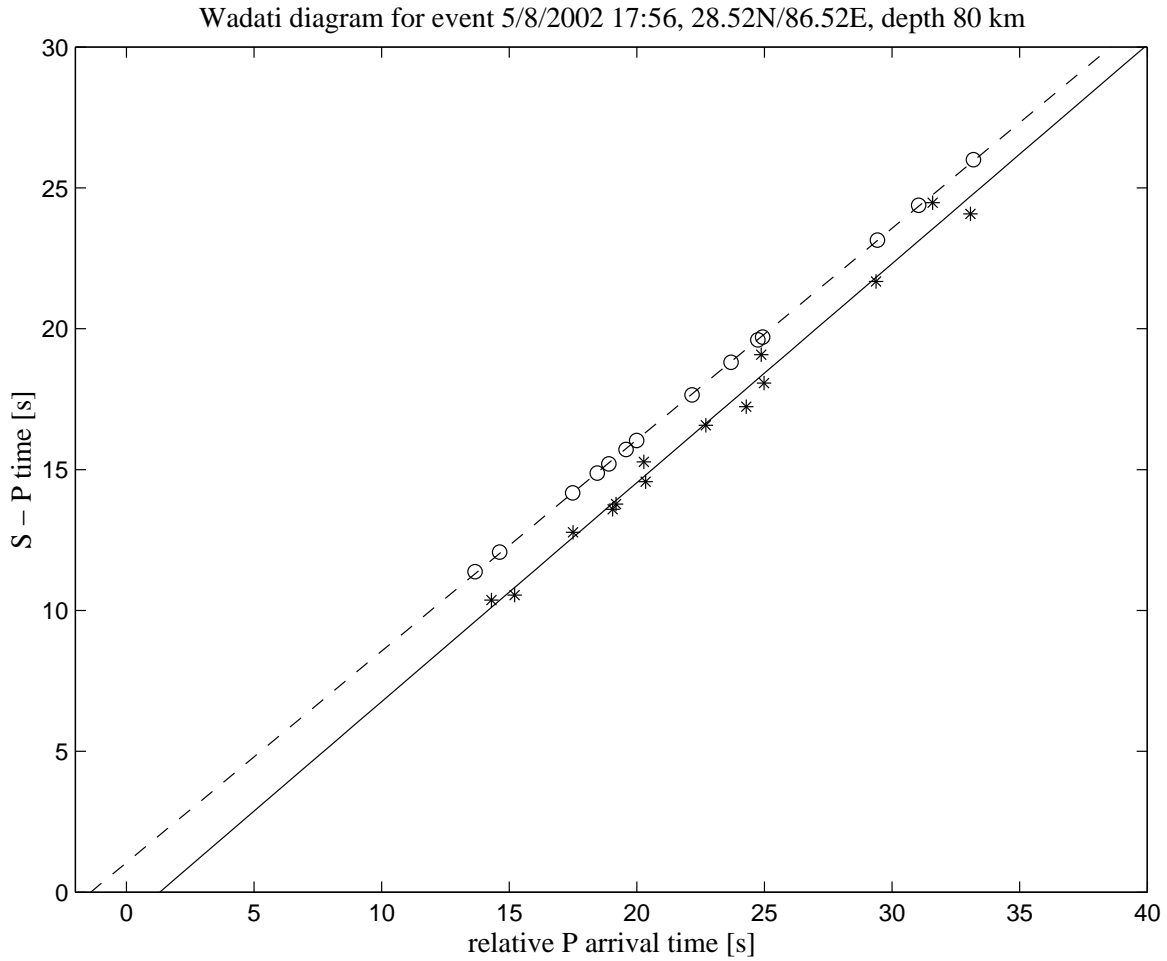
- [8] Avouac, J.-P. Mountain building, erosion, and the seismic cycle in the Nepal Himalaya. *Advances in Geophys.* **46**, 11–80 (2003).



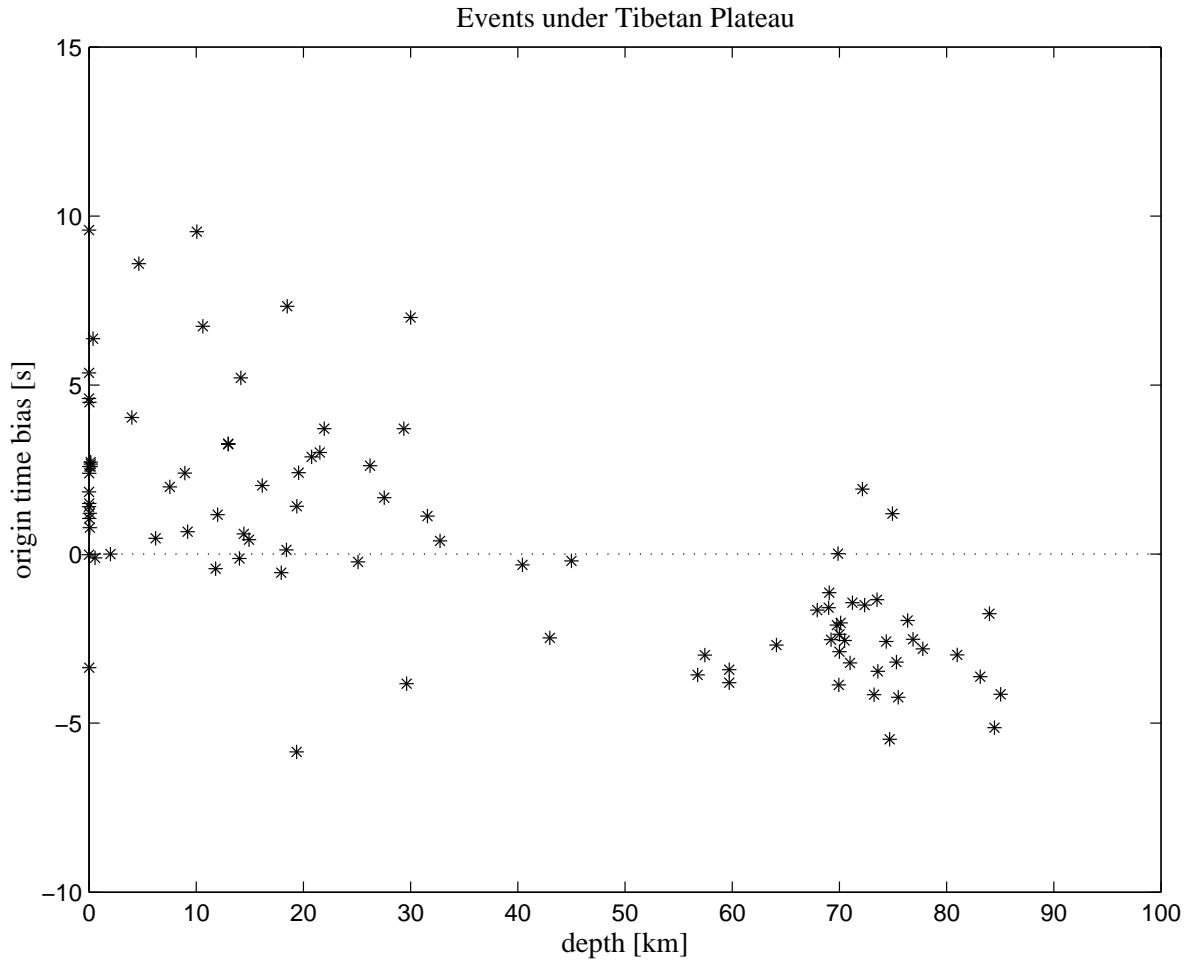
Supplementary Figure 1: Moveout plot for a limited azimuthal range at station BUNG. Overlaid curves are predicted moveout curves for a midcrustal interface at 20 km and a Moho at 45 km. Single conversions (positive polarity) are shown in as solid red, multiples with 2 P legs and one S leg (positive polarity) as black dash-dots, and multiples with two S and one P legs (negative polarity) are dashed blue. Matching the midcrustal multiples and Moho depths at nearby stations requires the introduction of a high-velocity anomaly above 20 km depth. (Moho multiples are unclear, possibly due to lateral heterogeneity.)



Supplementary Figure 2: Profiles calculated from eastern and western stations only to validate 2-D treatment of the entire data set. (top) Eastern stations on elevation profile, and common point conversion stack from their data. Lateral smoothing limited to 10 km. White areas are data gaps. (bottom) same for western stations. The features compare well between the eastern and western profiles, indicating that to first order, the arc-perpendicular variation in structure is negligible. Station SAGA (eastern outlier, in bottom panel, see Figure 1 in main paper for location) may show a slightly deeper Moho than other Tibetan stations near the suture zone, but the difference is within the vertical resolution limit dictated by the bandwidth of the receiver functions.



Supplementary Figure 3: Wadati diagram for a deep event under the Tibetan Plateau. Stars - picked arrival times; solid line - least squares fit to picked arrival times; circles - theoretical arrival times based on location using a previously published velocity model for southern Tibet [5]; dashed line - theoretical $S - P$ over P times based on location. See text for further explanation.



Supplementary Figure 4: Origin time bias of the minimum RMS residual solution for events under the Tibetan plateau using a previously published velocity model for southern Tibet [5]. Consistently negative biases for deep events indicate that the data require a faster lower crust than the model provides.